RICE UNIVERSITY

P-N Junction Photodetectors Based on Macroscopic Single-wall Carbon Nanotube Films

by

Xiaowei He

A Thesis Submitted
in Partial Fulfillment of the
Requirements for the Degree

Master of Science

Approved, Thesis Committee:

Junichiro Kono, Chair
Professor of Electrical and Computer Engineering and Physics & Astronomy

Robert H. Hauge
Distinguished Faculty Fellow in Chemistry

Kevin Kelly
Associate Professor of Electrical and Computer Engineering

Houston, Texas

November, 2012

ABSTRACT

p-n Junction Photodetectors Based on Macroscopic Single-Wall Carbon Nanotube Films

by

Xiaowei He

Single-Wall carbon nanotubes (SWCNTs) are promising for use in solar cells and photodetectors because of their strong optical absorption in most of the solar spectrum. There have been many reports about the photovoltaic effect in nanoelectronic devices based on individual SWCNTs, but they have been limited by complicated fabrication and miniscule absorption. Here we report the photovoltage (PV) and photocurrent (PC) in an easily fabricated macroscopic SWCNT film with a *p-n* junction, and we attribute these phenomena to the photothermoelectric (PTE) effect. Various factors affecting the PV amplitude and response time were studied, including the junction length, substrate, and doping level. We observed a maximal responsivity of $\sim$1 V/W with SWCNTs on Teflon tape, and a fast response time of $\sim$80 µs with SWCNTs on AlN substrates. We found that there exists a tradeoff between responsivity and response time based on the choice of substrate. It was found that the PV depended nonlinearly on the *n*-doping concentration, indicating the existence of an optimal doping level. Finally, we checked the photoresponse in a wide wavelength range (360–900 nm), and the PV was observed throughout, indicating that the device could potentially be used as a broadband photodetector.

Contents

Illustrations

Chapter 1

Introduction

Since their discovery by Iijima in 1991 [1], carbon nanotubes (CNTs) have been the focus of intensive investigation due to their unique one-dimensional (1D) structure and potential for application in a wide range of photonic and electronic devices [2–4]. In particular, the optical absorption of single-wall carbon nanotubes (SWCNTs) can be tailored to extend from the visible to infrared (IR) regimes by exploiting the polydispersity of their diameters, indicating their potential for application in solar cells and broadband photodetection.

Much of the early research about photoresponse of SWCNTs focused on their photoconductivity [5–20]. Unlike conventional bulk materials, the photoconductivity of SWCNTs is governed by complicated mechanisms, involving photodesorption of O_2 at the sample surface, sample heating by illumination (the bolometric effect), and the photovoltaic effect. The dominant mechanism varies with sample scale as well as experimental conditions. For individual semiconducting SWCNTs, photoconductivity in the IR is mainly due to the photovoltaic effect [8], while for large-area SWCNT films held under vacuum at low temperature, the photoconductivity is primarily due to the bolometric effect [13]. In microscopic SWCNT films held under vacuum with ultraviolet (UV) illumination, photodesorption of molecules happens on the sample surface, playing an important role in the change of conductivity [5].

Photovoltage (PV) generation in individual carbon nanotubes was first observed by Freitag *et al.* while taking photoconductivity measurements. They attributed the

PV signal to dissociation of photo-generated excitons [8]. This report has led to an explosion of research on PV and unbiased photocurrent (PC) measurements in individual semiconducting SWCNT devices [21–26]. In many of these experiments, exciton dissociation was achieved either by construction of Schottky barriers at a SWCNT-metal interface or by electrostatically-developed *p*-*n* junctions in the middle of a SWCNT. Although these devices generate PV by the photovoltaic effect (which is assumed to be fast and highly efficient), they are limited by their low absorption and thus cannot be used as commercial photodetectors.

There has been a growing trend for merging SWCNTs into micro and macroscopic devices to provide more practical applications, as the costs of SWCNT synthesis are expected to decrease [16–20, 27–34]. A photodetector device based on the combination of bulk CNT films and C_{60} has been constructed, demonstrating high external and internal quantum efficiencies of 2.3% and 44%, respectively [30]. However, this kind of device requires selection of specific semiconducting SWCNT chiralities to form a heterojunction with C_{60}, limiting optical absorption and increasing fabrication costs. PV and PC have been observed in suspended SWCNT films, which were generated by the photothermoelectric effect (PTE) at the SWCNT-metal interface [18]. These devices are easy to fabricate, but they usually have long response times ($\sim$10 ms) due to slow thermal diffusion of carriers [16–20]. While most studies on the PV of macroscopic SWCNT films have used randomly-orientated SWCNT networks, PV generation in a macroscopically aligned ultralong SWCNT film was recently reported by Nanot *et al.* [35]. Despite being driven by the PTE effect, it showed a fast response time on the order of microseconds by taking advantage of the high thermal conductivity of aligned SWCNTs.

In this thesis we investigate the photoresponse of macroscopic SWCNT films at *p*-

n junctions. Vertically aligned SWCNTs with length ∼60 µm were grown by chemical vapor deposition (CVD). After transfer to another substrate, an n-type film was created by liquid-based chemical doping with benzyl viologen (BV). The p-n junction was created by placing a p-doped film over the top of an n-doped film with a small overlap. Using 660 nm laser diode illumination, scanning PV microscopy measurements were performed on samples placed upon various substrates. These measurements revealed that a large PV was generated at the junction, which was an order of magnitude larger than the signal at the SWCNT-metal interface. The PV was very sensitive to substrate. On Teflon tape it reached a responsivity of ∼1 V/W with a slow response time on the order of seconds; on an AlN substrate it decreased to ∼0.05 V/W but with a fast response time of ∼80 µs. This result demonstrates the tradeoff between responsivity and response time based on choice of substrate. The PV also showed a strong dependence on doping level, indicating that dopant concentration could enhance the PV.

Chapter 2

Previous Work on Single-Wall Carbon Nanotube-Based Photodetectors

2.1 Studies of Photoconductivity in SWCNTs

Photoconductivity in conventional semiconductors arises from photogenerated electrons and holes being moved in opposite directions by an electric field. However, semiconducting SWCNTs are different from conventional bulk semiconductors in many ways. The photoconductivity of SWCNTs is more complicated than that of conventional semiconductors, being dominated by three main mechanisms: photodesorption, and the bolometric and photovoltaic effects.

Since SWCNTs are 1D wires consisting only of surface atoms, their physical properties are affected by surface effects. Photo-induced molecular desorption has been observed by performing photoconductivity measurements on an individual semiconducting SWCNT [5]. Using a UV light source ($\lambda = 254\,\text{nm}$) with an intensity of $2\,\text{mW/cm}^2$, it was found that the conductance G of the nanotube decreased by an order of magnitude. After turning off the light source, the conductance slowly recovered. When the same measurement was performed under vacuum (10^{-8} Torr), G decreased by three orders of magnitude with no recovery when the light was turned off. The result is shown in Figure 2.1. The change in photoconductivity is due to photodesorption of oxygen on the SWCNT surface.

Semiconducting SWCNTs appear p-doped in air because oxygen adsorbs onto their

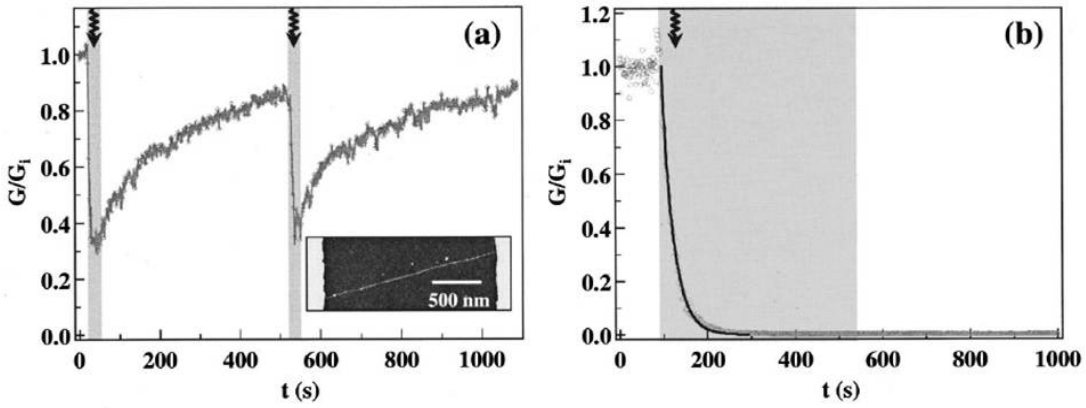

Figure 2.1 : (a) Normalized conductance of an individual semiconducting SWCNT vs. time during UV illumination cycles in air. (b) Conductance response to UV illumination in 10^{-8} Torr vacuum.

surface with a binding energy of $\sim$0.25 eV [13]. This process oxidizes the nanotubes by withdrawing one-tenth of an electron per oxygen molecule. Under UV illumination, oxygen photodesorption from the nanotubes causes a reduction of hole carriers, therefore lowering the conductance of the sample. However, when the light is turned off, gradual O_2 readsorption leads to the conductance returning to its original value. This is confirmed by performing the conductance measurement in high vacuum: After turning off the UV illumination, the conductance never returns to its pre-illumination level due to a lack of oxygen.

Photodesorption is highly wavelength dependent. It is pronounced under UV illumination but negligible under near-IR because the photon energy is too low to kick O_2 off the surface of the nanotubes. For macroscopic films containing a mixture of metallic and semiconducting nanotubes, photodesorption is important. The bolometric effect plays a dominate role in the photoconductivity of large area and suspended SWCNT films. The bolometric infrared photoresponse of suspended SWCNT films is shown in Figure 2.2 [13]. These films were held under vacuum at a temperature

of 50 K. It was found that the sample resistance decreased by 0.7% when placed under diode-generated IR radiation with an incident power of 0.12 µW and a peak wavelength of 940 nm. The same experiment was repeated with a SWCNT film on a substrate; no detectable change in resistance was observed. Taking into account the power level used in the experiment was five to ten orders of magnitude lower than in previously reported photoconductivity measurements, the suspension of the SWCNT film in vacuum led to an enhancement of the photoconductive response by five orders of magnitude. This change in resistance was interpreted as a bolometric effect.

In SWCNTs, photo-excite free electrons and holes quickly form strongly bound excitons; these excitons need to be dissociated thermally or by a large electric field to contribute to the photoconductivity. The exciton binding energy in SWCNTs is on the order of 0.5 eV and thus exciton dissociation is very difficult at room temperature (where $k_bT \approx 0.025\,\text{eV}$). At lower temperatures, thermal dissociation of excitons is substantially suppressed. For macroscopic SWCNT networks, the resistance is dominated by intertube junctions and thus very sensitive to temperature. In fact, these networks become more conducting when taken from low to high temperature. In the temperature regime where the localization dominates the conductivity, the resistance decreases exponentially with increasing temperature. When the thermal contact of a SWCNT film with environment is minimized by suspension, a considerable heating effect is expected in the film as the energy of the incident infrared radiation is efficiently transferred to the crystal lattice by electron-phonon interactions. Consequently, the temperature change in the sample leads to an observable change in resistance.

2.3

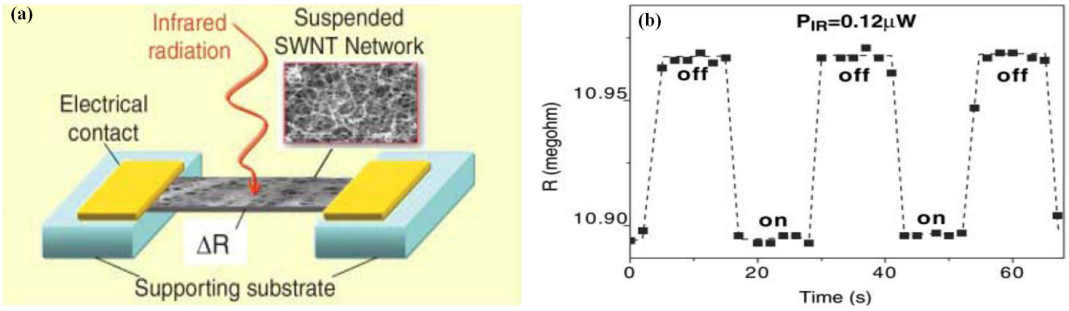

Figure 2.2 : (a) Diagram of a SWCNT network suspended between electrical contacts. (b) Modulation of resistance of a SWCNT film at 50 K under square-wave pulses of 0.12 μW IR radiation.

2.2 Photovoltaic and Thermal Effects in Individual SWCNTs and Randomly-Aligned SWCNT Networks

As discussed earlier, the photoconductivity of SWCNTs arises from multiple mechanisms. A purely photovoltaic effect involves exciton dissociation due to electric fields, and can be achieved by placing individual SWCNTs on a substrate, thus minimizing the photodesorption and bolometric effect.

The photovoltaic effect in a single SWCNT field-effect transistor (FET) was observed by Freitag *et al.* [8], in which a single semiconducting SWCNT was incorporated as the channel of an ambipolar FET shown in Figure 2.3(a). Proper treatment of the titanium carbide contact made the band lineup at the contacts approximately mid-gap, which allowed the device transfer from *p*-type to *n*-type under a back gate voltage, hence behaving as an ambipolar FET [36]. Optical measurements were performed with a continuous wave Ti:sapphire laser having a wavelength range of 780–980 nm and a typical power of $\sim$1 kW/cm^2. A moderate drain voltage on the order of 1 V was applied to separate excitons and collect carriers. A photocurrent of up to 100 pA was observed under illumination, while dark current was negligible as

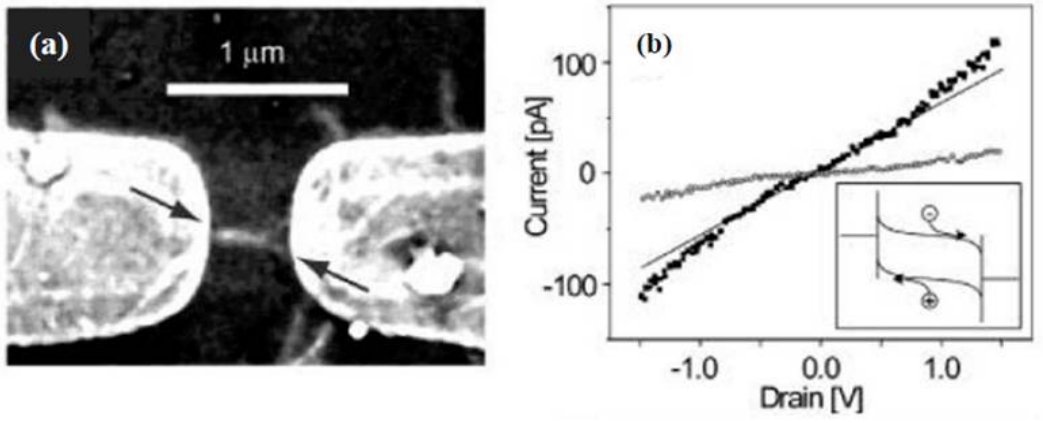

Figure 2.3 : (a) Scanning electron microscope image of a SWCNT FET. (b) Drain-voltage dependence of the current (○) without light and (■) with infrared light. (Gate voltage −2 V, IR intensity 5.6 kW/cm^2).

shown in Figure 2.3(b). Because the whole device was covered by a 10 nm layer of SiO_2, photodesorption was suppressed. In addition, since it only used a single tube placed directly on the substrate, sample heating by the bolometric effect was negligible. The observed PC was attributed to photon-induced exciton separation. The drain-bias dependence of the photocurrent showed nonlinear behavior above 0.8 V due to carrier tunneling in Schottky barriers from the electrodes in the nanotube channel.

This work indicated that Schottky barriers could contribute to PC by thermal emission. It opened the new area of study on photovoltage and unbiased photocurrent in individual SWCNTs in which Schottky barriers existing at electrode regions play the important role. After that, many papers were published showing that carbon nanotube FETs (CNTFETs) could generate PV and PC when illuminated with above-band gap light [21–26].

Under global illumination, CNTFETs do not usually show PV due to the existence

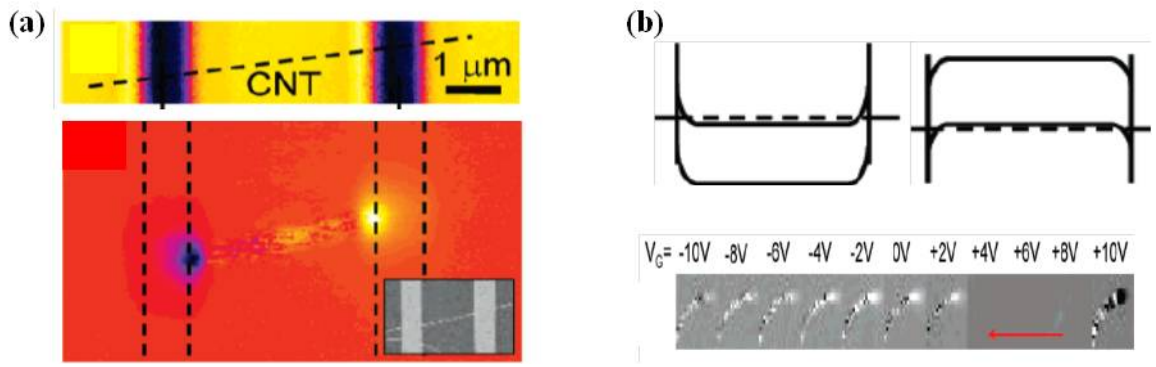

Figure 2.4 : (a) The top is a reflected light image from a laser-scanning microscope showing the two contacts of a CNTFET. The bottom is a short-circuit photocurrent image of the device under 500 µW of 457.9 nm laser excitation focused into a ∼0.4 µm spot. (b) Schematic of the band bending in n and p-type device as well as the ISC images of the contact region under various gate voltage.

of a mirror plane symmetry with respect to a plane perpendicular to the nanotube. This mirror plane symmetry can be broken by focusing the excitation spot to sub-device dimensions so that only a part of the nanotube is illuminated at a time. This technique has been used to demonstrate PV and PC induced by Schottky barriers in ambipolar CNTFETs [24]. Using argon laser illumination ($\lambda = 457.9\,\text{nm}$), a position sensitive PC was observed. Photocurrent only appeared when the light was focused on the interface between the CNT and metal electrodes, and it reversed sign when scanning from one electrode to another, as shown in Figure 2.4. Two effects were proposed to contribute to the observed photo signal: photons absorbed in the CNT channel produced excitons that were separated by the built-in electric fields in the barrier, and photons absorbed in the contact contribute through internal photoemission and thermally assisted tunneling. In addition, by changing gate voltage, the polarity of the Schottky barrier was able to switch from p to n-type. This transition led to PC changed sign in the same Schottky barrier which is shown in Figure 2.4.

Other than PC induced by Schottky barriers, more experiments were reported in which PC were driven by electrostatically induced *p*-*n* junctions in single CNTs [22, 25]. The common characteristic of all these experiments is that the device only includes one individual semiconducting CNT and the generation of PC is a purely photovoltaic effect. Although individual CNT devices are an ideal platform to study the fundamental properties of CNTs, they are limited by miniscule absorption and are far away from practical application. There has been a growing trend to merge SWCNTs into microscopic and macroscopic devices to provide more practical applications.

Recently, many studies of photo-detection devices based on large-area CNT films have been reported [16–20, 27–34]. For devices in which metallic and semiconducting CNTs have been isolated, the photovoltaic effect played the dominant role in generation of PV, while for devices in which metallic and semiconducting CNTs were mixed together, PV was primarily due to thermal effects.

Arnold *et al.* demonstrated that photo-generated excitons in semiconducting carbon nanotubes could be efficiently dissociated by forming a planar heterojunction between CNTs wrapped in semiconducting polymers and an electron acceptor; in this case C_{60} [30]. It is claimed that such a detector could reach peak external and internal quantum efficiencies of 2.3% and 44%, respectively. PC has been observed from 400 to 1450 nm with a response time of 7.2 ns. There are two reasons for such high efficiency and quick response time: First, a polymer (MDMO-PPV) has been used to isolate metallic nanotubes from optically active semiconducting nanotubes, thus minimizing their direct electronic coupling that could quench the photo-generated excitons. Secondly, the introduction of C_{60} allows for the formation of a type-II heterojunction between semiconducting nanotubes and C_{60}, in which the conduction band offset is

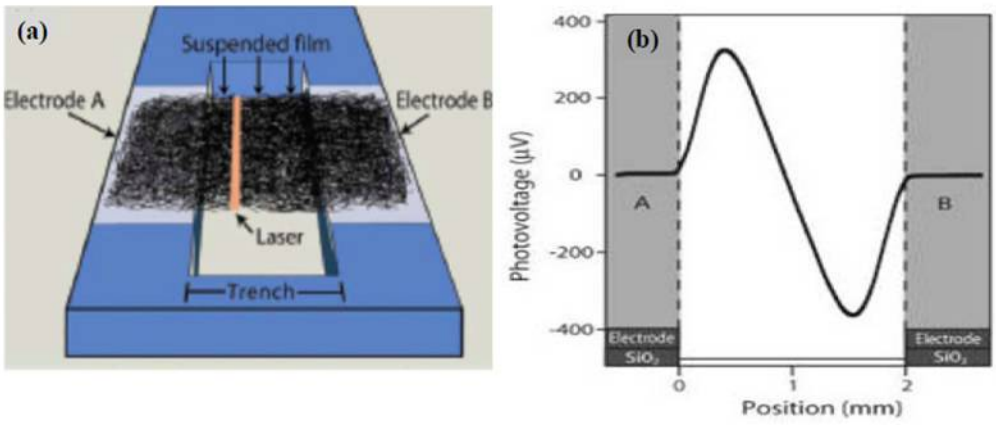

Figure 2.5 : (a) Illustration of the device consisting of a free-standing film bridging a 2 mm trench and illuminated by a laser. (b) PV profile of suspended SWCNT films as a function of laser position.

comparable with the exciton binding energy and thus efficiently dissociates them into electron-holes pairs.

Thermally-driven PV of suspended and mixed SWCNT films with macroscopic size was reported by St-Antoine *et al.* [18]. Figure 2.5 shows the result of a scanning PV measurement. PV signal only appears at the interfaces between SWCNTs and two electrodes. It looks similar to PV measurements in individual CNTFETs. However, the underlying mechanism is a thermal effect rather than a photovoltaic effect. Because of the mixture of metallic and semiconducting nanotubes, photon-induced excitons are strongly quenched and hardly contribute to the PV signal. The observed signal originates from the temperature difference between the two electrodes cause by local heating due to laser illumination. This is called the Seebeck effect, which we will talk more about later.

2.3 Photovoltage and Photocurrent in Aligned SWCNT Films

As discussed earlier, most previous works on PV and PC in SWCNT devices used individual SWCNTs or random networks of nanotubes in which the transport of carriers needs to conquer tube-tube junctions and therefore takes no advantage of the high-mobility character along the nanotube axis. The work of Nanot *et al.* first demonstrated photocurrent generation in macroscopically aligned ultralong CNTs [35]. The photodetector device was fabricated using a thin film consisting of dense arrays of ultralong (300 µm), aligned SWCNTs, grown by CVD, with two large, top-contacted electrodes as shown in Figure 2.6(a). With light from a 660 nm laser diode, scanning photocurrent microscopy revealed that most of the photocurrent was generated near the electrodes and changed the sign from one electrode to another [Figure 2.6(b)]. Different metals have been used as electrodes, but it has been found that Ti-deposited electrodes gave a maximal signal. The signal showed obvious polarization dependence because of the strong alignment of the SWCNTs; it is linearly dependent on the illumination power. The maximal photoresponse was on the order 0.1 V/W or 100 µA/W with response time on the order of 1 µs.

A theoretical model based on the Seebeck effect has been developed to interpret the observed photosignal. The basic assumption is that the Seebeck coefficient along the SWCNTs is position dependent: It undergoes a sharp change at the interface between electrode and SWCNT, but away from the interfaces it remains constant. A thermal voltage can be produced by a large Seebeck coefficient gradient with a position dependent temperature profile. It was applied to Nanot *et al*'s work and gave a reasonable agreement with the experimental results. This theoretical model

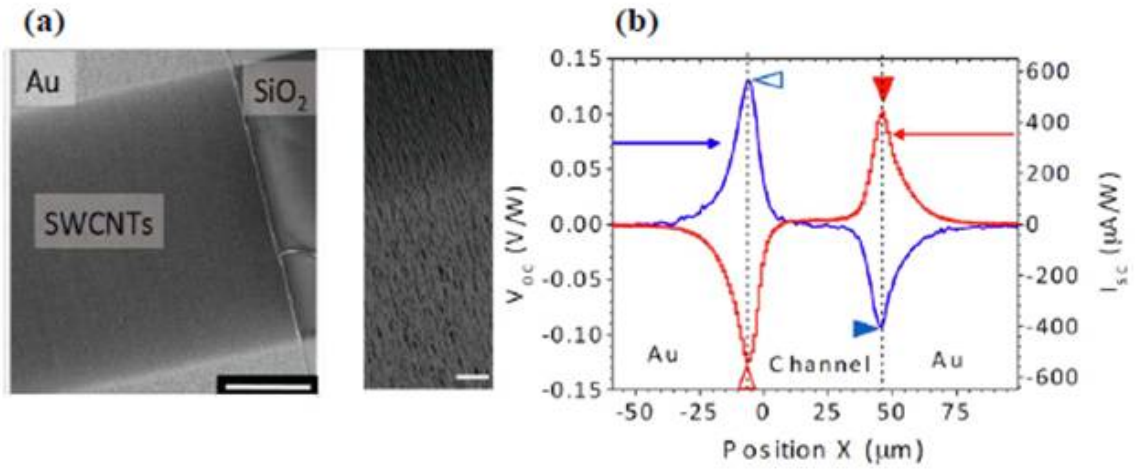

Figure 2.6 : (a) Scanning electron microscope image of aligned SWCNTs grown by CVD and transferred to SiO_2/Si substrate. (b) PV and PC profile as a function of position between two electrodes.

will be discussed in detail later in the present work about photoresponse on *p*-*n* junctions of SWCNT films.

Chapter 3

Growth of Aligned SWCNTs

3.1 Growth Equipment and Growth Principles

Carbon nanotube growth is a basic aspect of SWCNT-based photodetector research. There are several techniques for SWCNT growth, including laser ablation, arc discharge, high pressure carbon monoxide, and chemical vapor deposition (CVD). CVD is the best method for growing vertically aligned SWCNTs [37].

Shown in Figure 3.1 is our CVD setup. It consists of a tube furnace in which a 0.25 mm tungsten filament is suspended inside of a quartz tube. The role of the filament is to reduce the catalyst particles from oxidized states to metallic states. An MKS mass flow controller is used to control the precursor gases. A turbopump is used to keep the whole system under high vacuum ($\sim 10^{-6}$ Torr) when precursor gases are off.

Regardless of growth technique, the mechanism of CNT growth is expected to be universal [38]. This is depicted in Figure 3.2. At the proper temperature, hydrocarbons decompose on the surface of the metal catalyst. Then individual carbon atoms can diffuse along the surface to reach the growth site. Once they arrive at vacant sites in the carbon nanotube, they are incorporated into the lattice. The carbon nanotubes become longer while the hydrocarbon precursor gases flow. However, the catalyst particles stay at their original position on the supporting layer. This is called *root growth*.

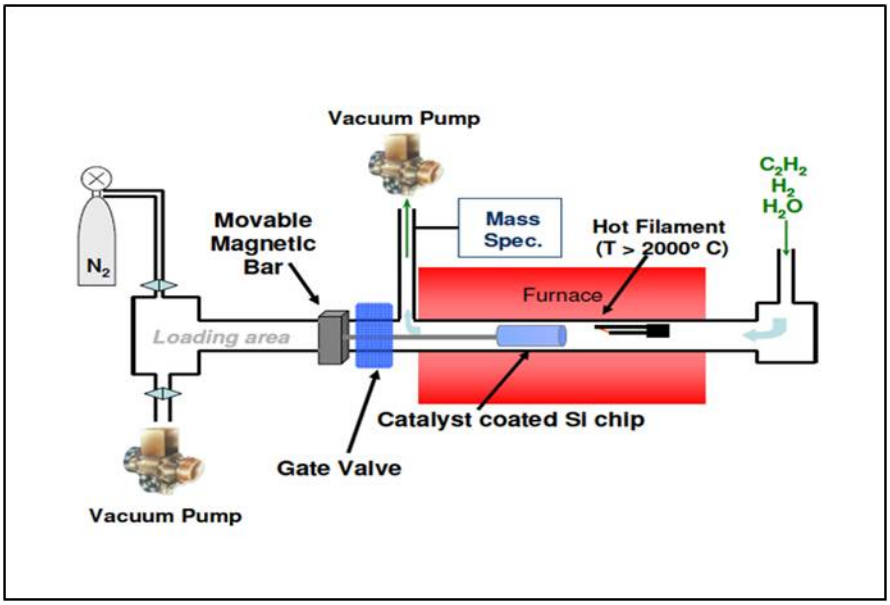

Figure 3.1 : Schematic of the hot filament CVD reactor

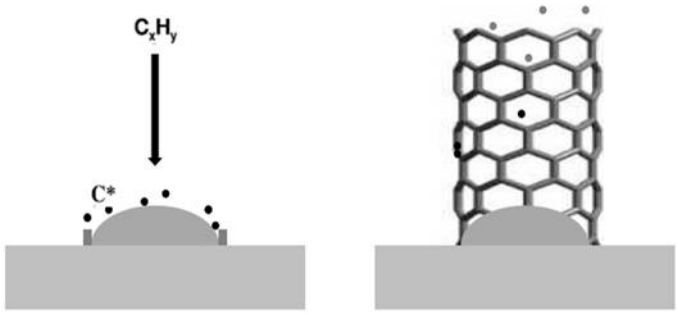

Figure 3.2 : Root growth of a vertically aligned SWCNT.

3.2 SWCNT Growth Procedure

A few steps are taken for vertically aligned SWCNT growth. The first is substrate preparation. The key point is the double layer structure of the substrate, a catalyst layer and a catalyst support layer [39]. Fe is used as the catalyst and Al_2O_3 is used as the catalyst supporting layer. First, an Al_2O_3 layer of thickness 10 nm is deposited on a Si substrate by electron-beam evaporation. Then a 1 nm layer of Fe is deposited on the Al_2O_3 by the same technique. The typical pressure during electron-beam evaporation is 3×10^{-6} Torr. The deposition rate is 0.5 Å/s for the Al_2O_3 and is 0.1 Å/s for the Fe layer [37].

After deposition, the $Si/Al_2O_3/Fe$ substrate is transferred to the CVD furnace. First, the furnace temperature is increased to 750 °C. Then, 200 standard cubic centimeters (sccm) of H_2, 4 sccm C_2H_2, and 200 sccm H_2 with water vapor are sent into the furnace. Water vapor is introduced in the system by bubbling H_2 through Nanopure H_2O. The tungsten filament is heated by ramping to a current of ∼9 A while precursor gases are flowing. When the power applied to the filament is stabilized around 35 W, the gate valve is opened and the sample holder is moved to a point that is approximately 2 mm from the filament. The filament causes reduction of the catalyst from Fe_2O_3 to catalytically active Fe. Then, SWCNT growth begins upon addition of the precursor gases to the CVD chamber. After growth, samples are usually checked under a JEOL 6500 scanning electron microscope (SEM). Figure 3.3 shows typical SEM images of vertically aligned samples after 3 minutes of growth with a height of ∼70 µm.

It is necessary to mention the function of water vapor flow during growth. First, it can hydroxylate the surface and makes it less likely for Ostwald ripening of catalyst particles [40]. Second, it cleans the SWCNTs by etching amorphous carbon that

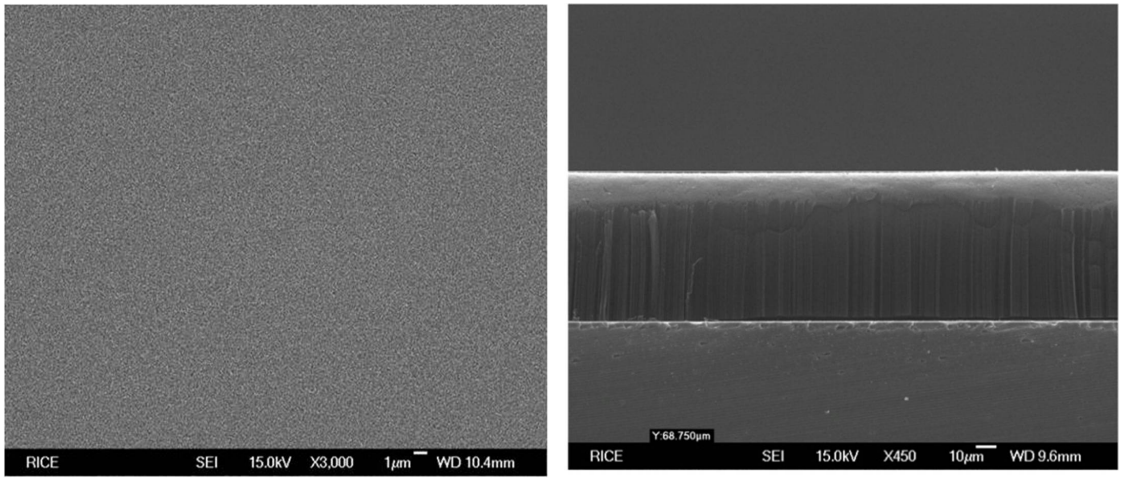

Figure 3.3 : SEM image of surface and cross-section of vertically aligned SWCNTs after 3 minutes growth.

covers the catalysts and tends to terminate the growth [27].

3.3 *p*-*n* Junction Fabrication

3.3.1 Sample Transfer

For both applied and fundamental research, it is important to transfer SWCNTs between different substrates and make thin films. The transfer process has been well-developed by Pint [37]. Because sample transfer is also an important step in our *p*-*n* junction film fabrication, in this section we talk about its mechanism and techniques in detail.

when carbonaceous gases flow over the Fe surface, they form a carbon coating consisting of Fe−C bonds. The nanotubes in the vertical arrays are fixed to the catalyst particles by strong C−C bonds to the iron-carbon coating. As a result, the nanotubes are difficult to transfer to other substrates. Therefore, the key to successful transfer is to destroy the Fe−C bonds. This can be achieved by a water

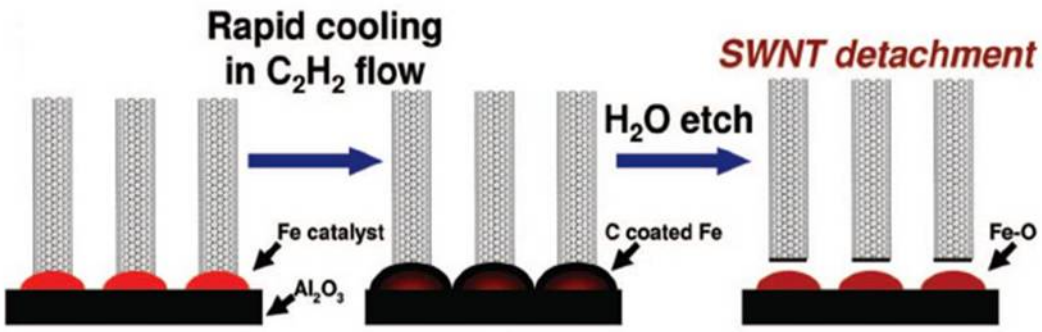

Figure 3.4 : Diagram depicting the water etching process after SWCNT growth

3.5

etching process (see Figure 3.5).

After water etching, the sample is ready to be transferred to an arbitrary substrate. First, the vertically aligned SWCNTs are pushed down horizontally on the growth substrate by using a smooth metal foil. Second, the growth substrate is flipped over and placed on a new substrate. A force is exerted on the back side of the growth substrate in order to ensure sample transfer. Removing the growth substrate leaves the sample attached to the new substrate. Surprisingly, such a transfer can keep the majority of alignment in sample. Figure 3.5 shows a typical SEM image of horizontally aligned SWCNT arrays after pushing the vertically aligned SWCNTs down on their growth substrate and transfer to Teflon tape. It shows that SWCNTs overlap and keep the same approximate direction, while the height has decreased from 70 µm to around 4 µm.

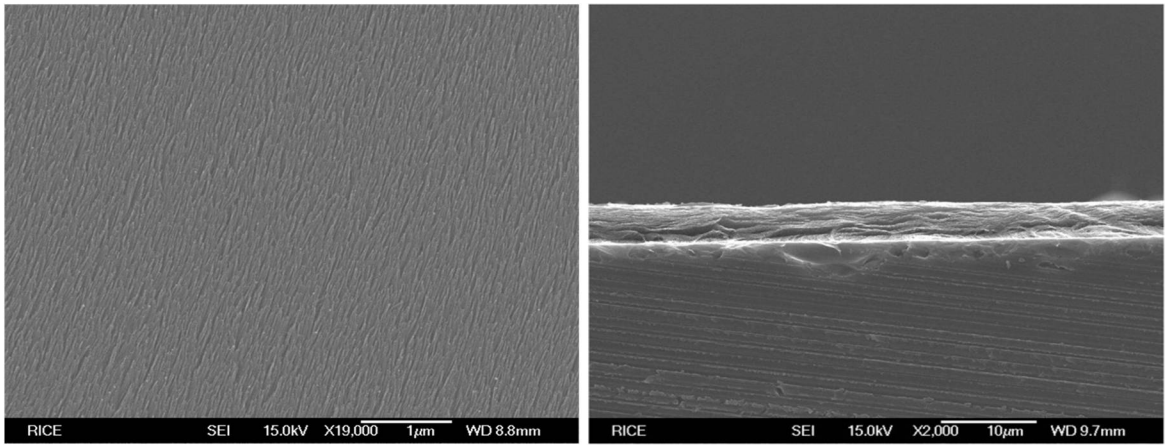

Figure 3.5 : SEM image of surface and cross-section of vertically aligned SWCNTs after transfer.

3.3.2 *n*-Doping SWCNTs by Benzyl Viologen

Doping conventional semiconductor materials has revolutionized the uses and applications of these materials in the past century. As a semiconductor with unique structure, the doping of semiconducting SWCNTs has received much attention. It is well-known that CNTs are *p*-doped when exposed to air because of O_2 adsorption [41]. So, in order to make *p*-*n* junctions in CNTs, it is necessary to find an efficient way of *n*-doping. It has been established that substitutional nitrogen doping into the CNT lattice is one way to create *n*-doped samples [42, 43]. However, this requires special growth equipment and relatively complicated techniques. Other than nitrogen doping, there are several non-substitutional *n*-doping methods such as alkali metal deposition and liquid-based chemical doping [44–47]. The essence of this type of doping is the charge transfer during the redox reaction that occurs when attaching dopants to the nanotubes. Among them, benzyl viologen (BV) doping is a simple, controllable, and very stable way to make *n*-doped CNTs [47].

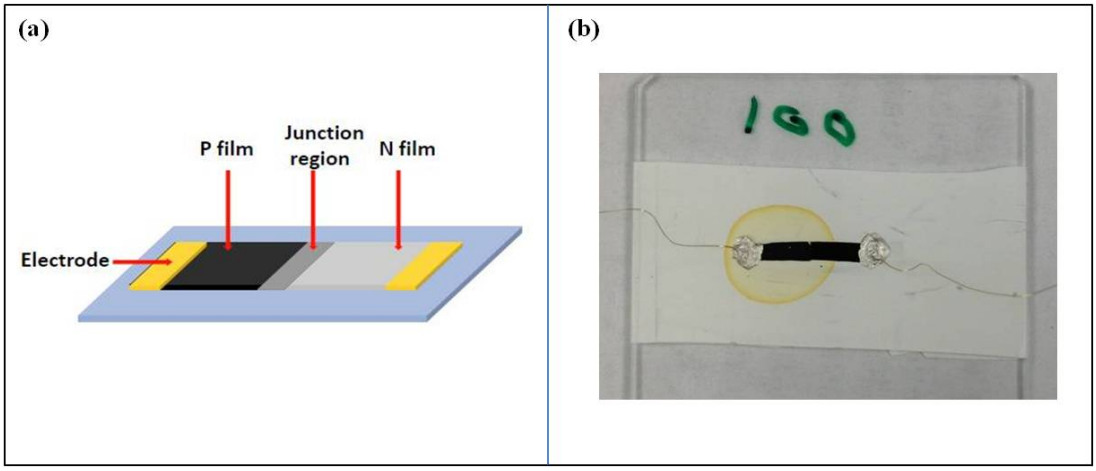

Figure 3.6 : (a) Diagram of the SWCNT device. (b) Photograph of the p-n junction sample on Teflon tape wrapped around a glass slide.

Following the procedure in [47], we use BV doping to make n-type SWCNT films. Since SWCNTs are naturally p-doped in air, we construct a p-n junction by overlapping an n-doped film with a naturally p-doped film. Figure 3.6 shows a cartoon and a real picture of a p-n junction sample on Teflon tape.

In order to make different sized p-n junction samples, we used multiple transfer techniques. Specifically, a vertically aligned SWCNT array with larger area (6 mm × 8 mm) on a Si substrate was transferred onto Al foil. Then the thin film attached on the surface of the Al foil was cut to the desired size. This small film was transferred to Teflon tape to make p-n junctions.

The final step in device fabrication was electrode deposition. It was done either by daubing silver paste or sputtering gold. Both techniques were used in our samples and gave a typical resistance of 50–150 Ω. The silver electrode was made by colloidal silver liquid from Ted Pella (Product number 16034), while the gold electrodes were deposited by CRC-150 sputter coater with a typical thickness of 50 nm.

Chapter 4

Photoresponse Measurements of p-n Junction SWCNT Films

4.1 Photothermoelectric Effect in SWCNTs

As discussed previously, the photothermoelectric (PTE) effect is the dominant mechanism governing the photoresponse of large-area SWCNT films with a mixture of semiconducting and metallic carbon nanotubes. We start by discussing the thermal voltage generated by thermocouples between CNTs and metal electrodes (see Figure 4.1).

From the general theory of the Seebeck effect, the thermoelectric potential is given by

$$V_R - V_L = \int_{T_R}^{T_L} S(T)\, dT \tag{4.1}$$

$$= \int_{x_R}^{x_L} S(x) \nabla T\, dx, \tag{4.2}$$

where $S(T)$ is the Seebeck coefficient of a CNT film at temperature T. The contribution to the thermopotential from the metal has been ignored because it is usually very small. For the case of SWCNT films where S is constant and the temperature profile is given by a constant gradient in the channel, we recover the usual expression $\Delta V = -S_{\mathrm{CNT}} \Delta T$. However, in the case of local illumination, the laser induced temperature profile is given by a peaked, symmetric profile, and if S is constant in the channel then the PV would be exactly zero. Therefore, to obtain a non-zero PV due

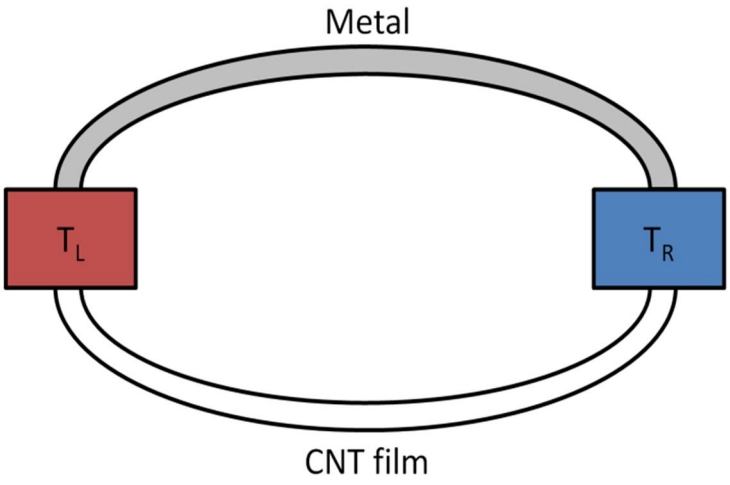

Figure 4.1 : Diagram of thermocouple between a CNT film and metal electrodes.

to the thermoelectric effect, we must necessarily have a position-dependent S. This can be made explicit by integrating (4.2) by parts to obtain

$$V_R - V_L = S_L T_L - S_R T_R - \int_{x_R}^{x_L} T(x) \frac{dS}{dx}\, dx. \tag{4.3}$$

Under local illumination, $T_L = T_R =: T$, so we can define $T_0 := T(x) - T$, so that (4.3) becomes

$$V_R - V_L = -\int_{x_R}^{x_L} T_0(x) \frac{dS}{dx}\, dx. \tag{4.4}$$

This implies that it is possible to generate a large PV by inducing a sharp change in S along the CNT channel. Theoretical calculations show that the Seebeck coefficient of semiconducting SWCNTs is a function of the Fermi level; this functional relationship is given by

$$S = -\frac{k_B}{|q|} \frac{I_1}{I_0} \tag{4.5}$$

where

$$I_j := -\int_{-\infty}^{\infty} \left(\frac{E - E_{\mathrm{F}}}{k_B T} \right)^j T(E) \frac{\partial f}{\partial E}\, dE \tag{4.6}$$

where k_B is the Boltzmann constant, T is the temperature, q is the electron charge, $T(E)$ is the electronic transmission through the SWCNT, f is the Fermi function, E_F is the Fermi energy, and E is the energy measured from the center of the nanotube band gap. In the flat band case, (4.6) can be integrated analytically to give

$$I_0 = 1 + f(E_C) - f(E_V) \tag{4.7}$$

and

$$I_1 = \left(\frac{E_C - E_F}{k_B T} \right) f(E_C) - \left(\frac{E_V - E_F}{k_B T} \right) + \ln \left[\frac{1 + \exp\left(-\frac{E_C - E_F}{k_B T} \right)}{1 + \exp\left(-\frac{E_V - E_F}{k_B T} \right)} \right] \tag{4.8}$$

where E_C and E_V are the energies of the conduction and valence bands, respectively.

The main information from (4.5) is that S is strongly sensitive to the position of the Fermi level in the bandgap and thus can be modulated by changing carrier concentration. This is illustrated by the diagram in Figure 4.2(a), where the sign of S changes from positive to negative when the CNTs change from p-type to n-type. If a p-n junction is introduced into the channel of the CNT film, there would be a sharp change of S which is shown in Figure 4.2(b).

Equation (4.4) shows that a nonvanishing gradient of S is necessary to generate PV in CNT films under local illumination. Nanot et al have demonstrated that a PV signal can be generated at the interface between sample and electrodes by a local change of S due to electrode doping [35]. Instead of electrode doping at the ends of a sample, if a p-n junction is made in the middle of a CNT film by chemical doping, we could expect a larger PV because of the sharper change of S at the junction. This is

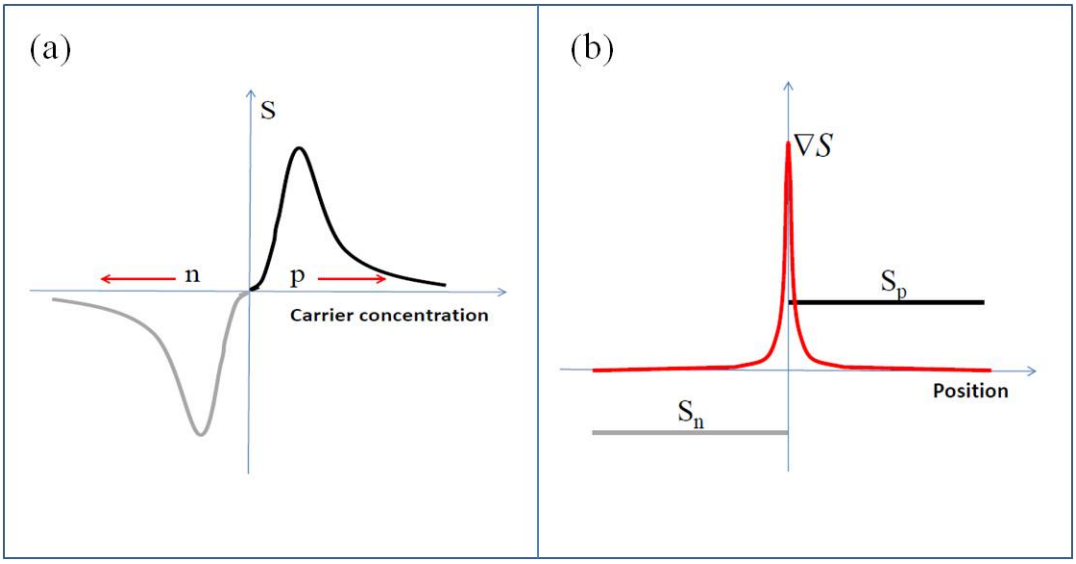

Figure 4.2 : (a) Plot of the Seebeck coefficient S as a function of carrier concentration. (b) Plot of ∇S due to a sudden change of S at the p-n junction.

our motivation to fabricate a PTE-based photodetector based on p-n junction CNT films.

4.2 Photoresponse Measurement on p, n, and p-n Junction SWCNT Films

Our experimental data was taken primarily by a home-built scanning photocurrent microscopy system (Figure 4.3). The light source was a 660 nm laser diode, which was focused to a diameter of ∼1 µm on the sample through a long working-distance apochromatic objective lens with a typical continuous wave power of ∼10 mW.

A white light source and a Si CCD camera were introduced into the system; their function was to locate the position of the laser beam on the sample. The sample was kept in an optical cryostat, but all current measurements were performed in air and

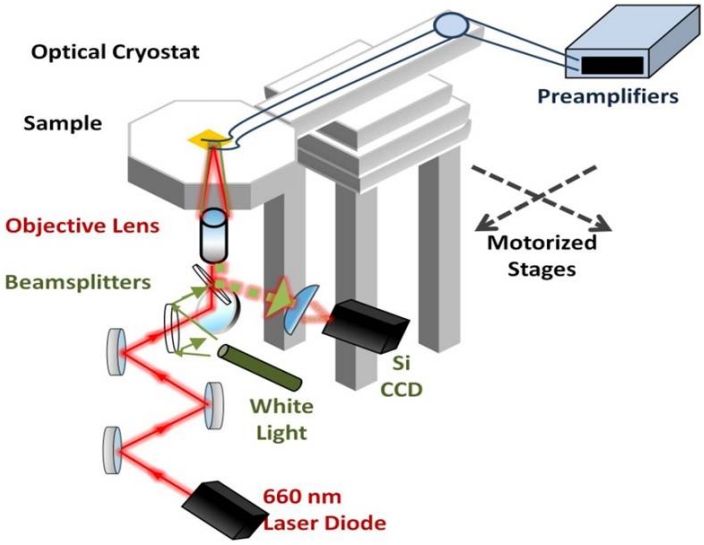

Figure 4.3 : Diagram of the home-built scanning photocurrent microscopy system.

at room temperature. The motorized stages which held the cryostat were controlled by a motion controller that allowed the stage to move along x and y-direction in the plane with a resolution of $\sim$1 µm. The photosignal from the sample was amplified by preamplifiers. An integrated LabView program was used to collect the signal and control the motion of the stage.

As described in Chapter 3, a p-n junction SWCNT film sample was grown by CVD, transferred to Teflon tape,and then n-doped by BV. Finally another p-doped film was transferred to Teflon tape and slightly overlapped with the n-doped film to make a p-n junction, which is shown in Figure 4.4. Besides the p-n junction sample, in order to make comparison we also prepared unintentionally p-doped SWCNT films and totally n-doped SWCNT films. The BV doping concentration for all n-doped samples was 50 mM. After focusing the laser beam on the sample with a power of

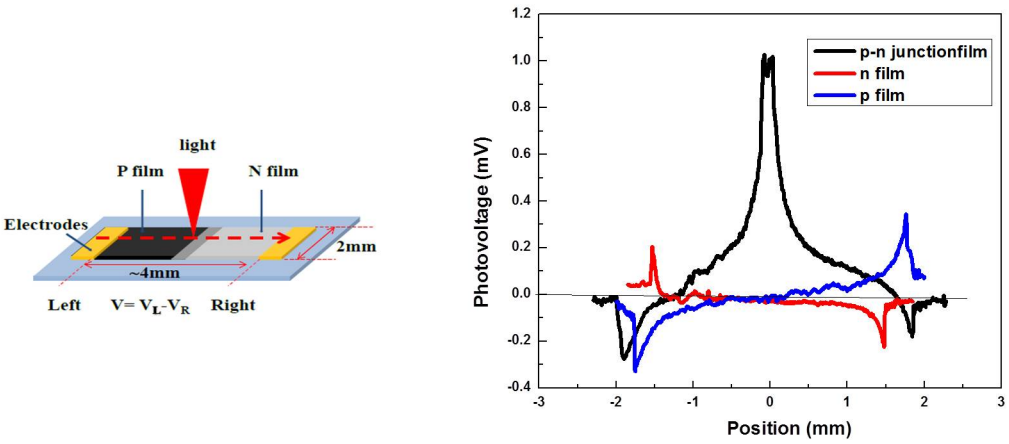

Figure 4.4 : Left: Diagram of the p-n junction device. Right: PV as a function of position between electrodes for n, p and p-n junction SWCNT films.

10 mW and beam diameter 1 µm, the optical scanning from the left to right side of the sample was done by using scanning microscopy system (see Figure 4.3). PV was always measured as the voltage at the left side minus the voltage at the right side, which is consistent with the scanning direction of the laser beam. Shown in Figure 4.4 is the position dependence of PV for all three types of samples. It has been observed for all kinds of samples but with totally different position dependence. For pure p- and n-doped samples, PV only appeared at the interfaces between sample and electrodes. The sign change of the PV can be observed from p- to n-doped samples. Based on the theory of the Seebeck effect, the hot end of a p-type sample has a lower voltage relative to its cold end because of a positive Seebeck coefficient. On the contrary, it has a higher voltage at hot end for n-type samples because of a negative Seebeck coefficient. This is fully consistent with our experimental results. When a laser heats the left side, the PV for the p-doped film is negative, which means that V_L is lower

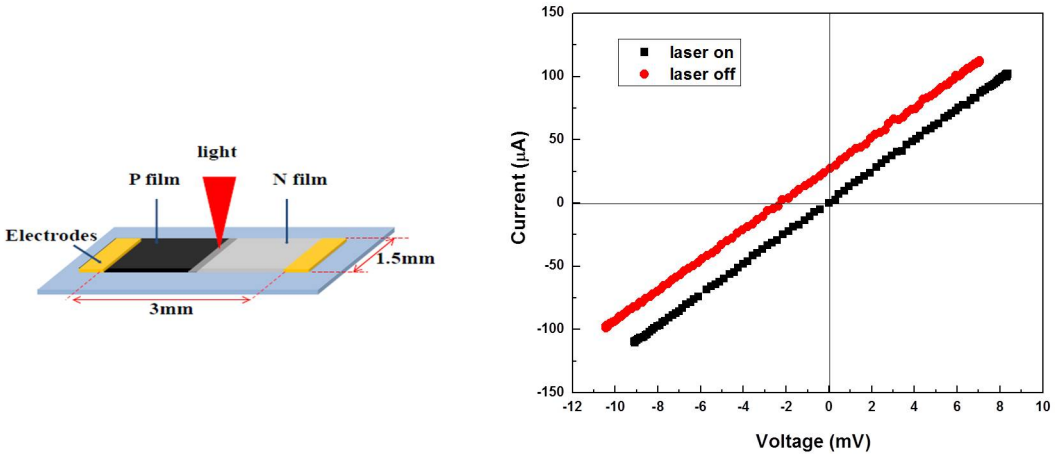

Figure 4.5 : I-V curve of a p-n junction SWCNT film with and without illumination. (The inset shows the diagram of p-n junction devices)

than V_R, while the positive PV for n-doped films means that V_L is higher than V_R. When the laser beam moves to the right side, the hot end is reversed, and PV changes sign accordingly.

A $+1\,\mathrm{mV}$ PV was observed at the junction region for p-n junction samples, three times larger than signals at regions close to the two electrodes (see black curve in Figure 4.4). The signal can be explained by the sharp change of S at the junction region. From the left side to the right side, the film undergoes the change from p type to n-type, and correspondingly, S suddenly changes sign from positive to negative, leading to a large negative ∇S at the junction. Consequently, as implied in (4.4), this negative ∇S in the middle of the sample channel contributes a positive PV when heated by local illumination.

In order to fully check the photoresponse of p-n junction samples, we also did I-V measurements. A typical result of an I-V measurement with and without laser

illumination at the junction is shown in Figure 4.5. An obvious shift of the I-V curve can be observed with the laser on, indicating there is an unbiased photocurrent. PC and PV estimated from the shift of the I-V curve is $\sim$25 µA and $\sim$2 mV, respectively. The I-V curve shown in Figure 4.5 is very linear, though there is a p-n junction in the middle of the SWCNT film channel. This is not surprising considering that CVD grown samples are always a mixture of semiconducting and metallic SWCNTs,and the existence of metallic SWCNTs provides shorting channels in the p-n junction region. The linearity of the I-V curve shows that PV in the sample is due to thermal effects and not the photovoltaic effect. In addition, from the slope of the I-V curves in Figure 4.5, it can be found that the resistance of the sample is around 80 Ω and is unchanged by illumination. This indicates that photodeposition and bolometric effects in our sample are negligible.

Based on above experimental results, we come to three conclusions. First, CNT films realize the transition from p-type to n-type and S reverses its sign by BV doping. Second, it proves that a large PV can be generated inside a SWCNT film channel by fabricating a p-n junction. Third, PV generated in a p-n junction region is due to the Seebeck effect rather than the photovoltaic effect.

4.3 Factors that Affect the Photoresponse of p-n Junction SWCNT films

4.3.1 The Effect of p-n Junction Overlapping Region on PV Generation

Because the p-n junction sample was made by overlapping one n-doped SWCNT film with another p-doped film, it actually consisted of three parts: two edges and a narrow overlapping region. In order to figure out which part the observed signal

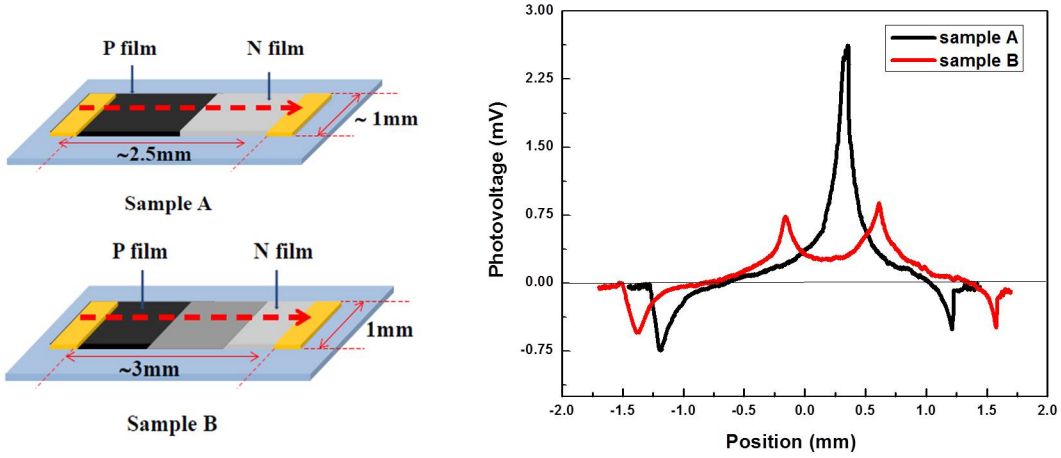

Figure 4.6 : Left: Diagram of sample A and sample B. Right: PV as a function of position between electrode for sample A and sample B.

came from, two samples were made to make comparisons, which are shown by the cartoon in Figure 4.6. Sample A and sample B had the same growth time, and n-type SWCNT films were doped by BV solution with concentration 70 mM. A very sharp p-n junction was made in sample A, but overlapping distance of p-n junction for sample B was very long with length $\sim$1 mm.

Scanning PV measurements were performed on the two samples with the same illumination power of 10 mW. Figure 4.6 shows the PV position dependence for the two samples. One can find that there is only one peak appearing at the junction of sample A, but two peaks appear for sample B, exactly located at two edges of the p-n junction. In the overlapping region, PV become smaller compared with two edges. This means most of the signal comes from the edge instead of the overlapping region. Furthermore, the PV amplitude of two peaks from sample B is much smaller than the one in sample A, indicating that the overlapping region suppresses the ability of

signal generation rather than enhancing it.

This experimental result is explained by taking into account the large thermal diffusion in our samples. From PV profiles in Figure 4.6, it can be estimated that the thermal diffusion length in both samples approaches 1 mm; this is mainly due to the small thermal conductivity of Teflon tape. The thermal diffusion length is on the order of a millimeter, but the sample thickness is just 3–5 µm, therefore the temperature change along the perpendicular direction is negligible. Consequently, carriers rarely cross the p-n junction to diffuse in the perpendicular direction when illuminating on the overlapping region, and thus PV is mainly generated by carrier diffusion along the in-plane direction. Considering the overlapping region, hot electrons and holes diffuse in opposite directions in the plane, and so they tend to compete with each other. So, it behaves like an intrinsic semiconductor that has a constant S around zero theoretically, leading to zero PV when illumination is in the overlapping region. However, if light is focused at the two edges, S undergoes a sudden change from n or p-type film region to overlapping region, leading to the observable PV. That is basically the situation we observed in sample B. The non-zero signal in the overlapping region of sample B is nothing more than a tail effect from two edges because of the long thermal diffusion length. For sample A, because the length of overlapping region is negligible, the junction can be considered as a sharp connection between a pure p-doped film and n-doped film, resulting in one peak at the interface. It is necessary to mention that the peak signal of sample A is much larger than sample B; in fact, even larger than the sum of the two peaks from sample B. This is because PV at sample A is contributed by S changing from pure p-type to pure n-type, and it is much larger than the S change from pure p or n to the overlapping region in sample B.

According to above experiment results, we conclude that PV is only generated

at the edges of the p-n junction. The overlapping region behaves like an intact SWCNT film with a very small S because of the lack of temperature gradient along perpendicular direction.

4.3.2 The Effect of Different Substrates on PV Response Time and Amplitude

As discussed before, PV in p-n junction SWCNT samples is driven by the Seebeck effect. One can expect that signal generation could be very sensitive to substrate due to heat dissipation by the substrate. So, in this section, we check the effect of substrate on photoresponse of the p-n junction SWCNT samples.

We start by discussing the heat transport for a SWCNT film with thickness h and width W, which is put on a substrate and placed under local illumination. The heat equation is given by

$$hW\kappa\nabla^2 T - WG_s(T - T_s) = p\delta(x - x'), \tag{4.9}$$

where T is the temperature, κ is thermal conductivity, G_s is thermal conductance between the film and the substrate, and T_s is the temperature of the substrate. In this equation, heating by the laser is modeled as a point heat source of strength p at x'.

The solution of (4.9) for $\Delta T := T(x) - T_s$ is

$$\Delta T(x, x') = \frac{p}{G_s \lambda W} e^{-|x-x'|/\lambda}, \tag{4.10}$$

where λ is the thermal diffusion length given by

$$\lambda = \sqrt{\frac{\kappa h}{G_s}} \tag{4.11}$$

From (4.10) and (4.11), it can be found that the temperature gradient ΔT is inversely proportional to $\sqrt{G_s}$, while we know that the thermal potential is proportional to ΔT from (4.4). Consequently, we get that PV is inversely proportional to $\sqrt{G_s}$, which indicates that the larger the thermal conductance between sample and substrate, the smaller the amplitude of PV. Physically, it means that the signal induced by sample heating is weakened because of heat dissipation through substrates. This is why Teflon tape is chosen as the sample substrate. It has a very low thermal conductivity of 0.17 W/mK, so that heat is difficult to dissipate to the environment, leading to a strong increase in local temperature in the sample, and thus, a strong PV. In order to study the effect of substrate, measurements were performed on the same sample with different configuration but same illumination power of $\sim$10 mW, which is shown in Figure 4.7. In the first configuration, same with the previous measurement, the sample was on Teflon tape and wrapped around glass slides. In second configuration, the sample was on Teflon tape but without support of glass slides.

Shown in Figure 4.7 is the experimental result. It can be found that the PV profile is broadened in the free-standing situation (without the glass slide), while it becomes narrow with glass support. The broadening of the PV profile implies an increase of the thermal diffusion length. From Figure 4.7, it can be estimated that the thermal diffusion length is above 1.5 mm. The shrink of thermal diffusion [see (4.11)] is due to the suppression of thermal conductance when the sample is free-standing. Furthermore, the peak value for the free-standing situation is also larger than that in the supporting situation. This is because laser heating becomes more efficient by quench of heat flow to the environment, and a larger increase in temperature in the sample leads to a larger PV.

In order to further study the effect of substrates, PV for samples on AlN substrates

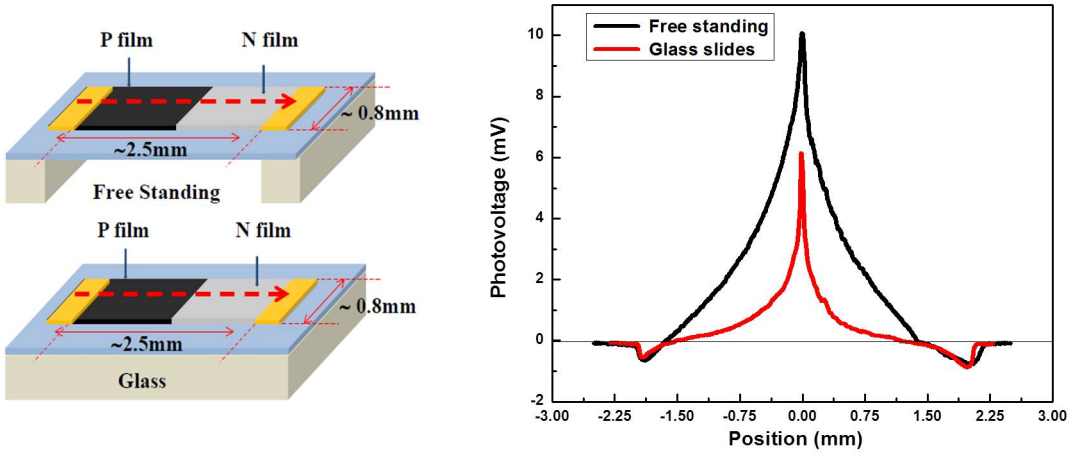

Figure 4.7 : Left: Diagram of sample one is on glass slide and the other is without glass slide, the blue layer indicates Teflon tape. Right: PV as a function of position between two electrodes for two different configurations.

were measured. A SWCNT film was transferred to an AlN film with thickness 1.5 mm. AlN was chosen as a substrate because it is a good thermal conductor with thermal conductivity ∼140–180 W/mK. Scanning PV measurements from the left side of the sample to the right side were performed under the same illumination conditions as before.

As seen from Figure 4.8, the PV profile becomes much sharper as compared with previous measurements, and the thermal diffusion length decreases to around 0.25 mm. The peak value of PV is around 0.5 mV, which is decreased by more than one order of magnitude compared with the free standing situation. Since AlN has a very high thermal conductivity, it becomes an efficient heat sink when the sample is heated by laser illumination. Consequently, the increase in sample temperature by laser heating is suppressed, leading to the decrease in PV. The thermal diffusion

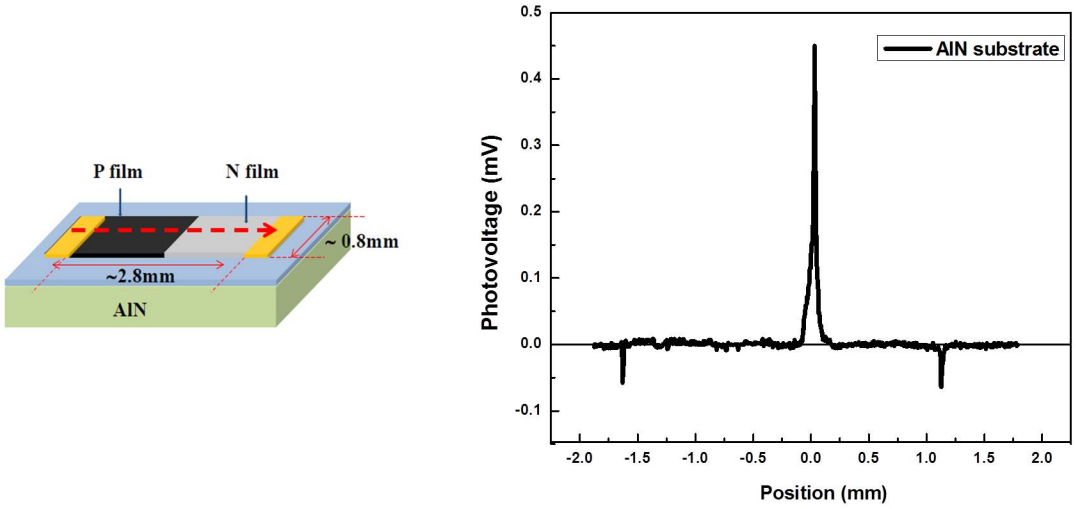

Figure 4.8 : PV as a function of position between two electrodes for the sample on AlN substrate. The left shows the diagram of the sample with AlN substrate.

length strongly shrinks due to the large enhancement of thermal conductance between the SWCNT film and substrate, leading to an extremely sharp peak at the interface between the p and n-doped film.

The change of substrate does not only affect the amplitude of the PV but also affect its response time. By suddenly moving an opaque board into and out of the light path, the square-wave pulses of laser illumination were introduced into the system, allowing us to study the PV response of the sample with different substrates. The comparison of PV response between AlN substrate and Teflon tape is shown in Figure 4.9(a). One can find that the PV amplitude is much smaller but its response is quicker for the sample on the AlN substrate compared with one on the Teflon substrate. In order to clearly show the difference of response time for different substrates, PV amplitudes have been normalized to the same value in Figure 4.9(b). For the sample on Teflon

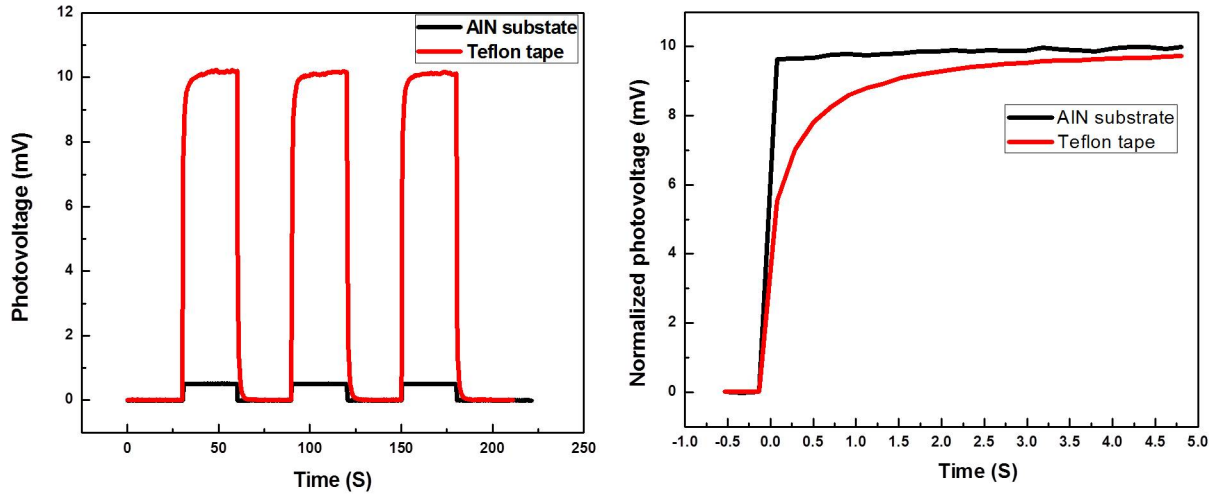

Figure 4.9 : (a) Modulation of PV for sample with different substrate under square-wave pulses of illumination, the red and black curve show the PV of sample on Teflon and AlN, respectively. (b) The comparison of PV response time between Teflon and AlN substrate after amplitude normalization.

tape, it takes a few seconds to reach the maximal signal, but for the sample on AlN substrate, it quickly reaches the maximal signal; in fact, the response is beyond the resolution of the measurement apparatus.

In order to measure the response time for the sample on AlN substrate, an oscilloscope and chopper were used. A periodic PV signal was induced by the chopper with a frequency of 700 Hz and was monitored by an oscilloscope. Figure 4.10 shows the increase and decay of PV with the laser on and off, respectively. Exponential fitting gives response times of $\tau_{\text{on}} \sim 90\,\mu\text{s}$ and $\tau_{\text{off}} \sim 84\,\mu\text{s}$, respectively.

The above experiment demonstrates that quick response times can be achieved by choosing a good thermal conductor as a substrate but at the cost of signal amplitude. This can be understood by taking into account the time scale of the temperature

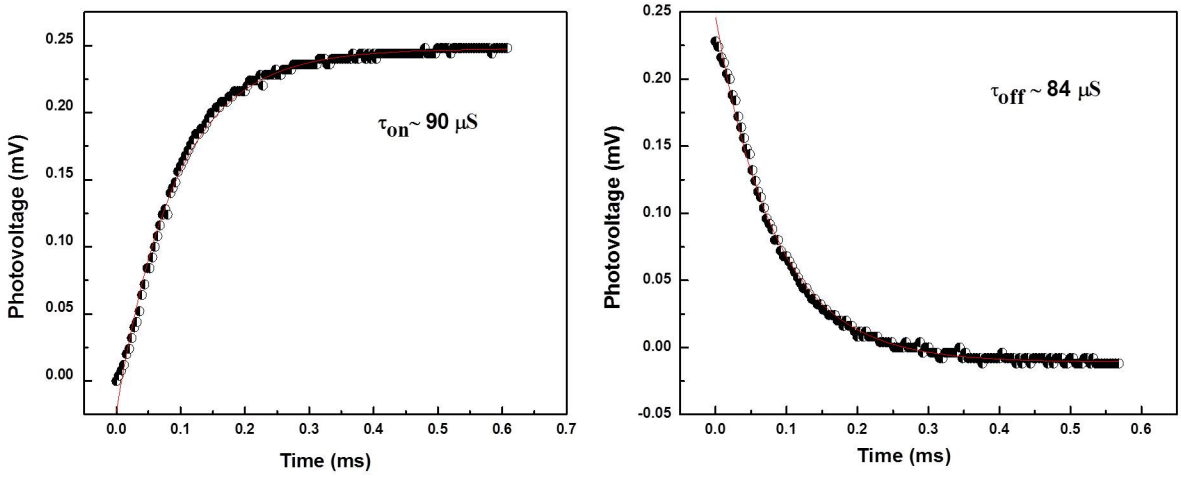

Figure 4.10 : (a) PV response time of sample on AlN substrate when laser is on. (b) PV response time of sample on AlN substrate when laser is off. (Dark dots indicate experimental data, and red curves indicate fitting results.)

profile developed in the system. Because PV is dependent on the development of a temperature profile in the sample, the faster the building of the temperature profile, the quicker the response time of the PV. For a substrate with good thermal conductivity, heat flow is fast and it quickly reaches thermal equilibrium and therefore gives a quick response time.

Consider the time-dependent heat equation,

$$hW\rho C_p \frac{dT}{dt} = hW\kappa\nabla^2 T - WG_s T, \tag{4.12}$$

where ρ is the film mass density and C_p is the heat capacity. Starting from the profile in (4.10) at $t = 0$, the time-dependence of the maximum temperature can be obtained from

$$T_{\max} \approx \frac{p}{G_s W} e^{-t/\tau} \tag{4.13}$$

where the time scale τ is given by

$$\tau = \frac{h\rho C_p}{G_s} \tag{4.14}$$

It can be found that the response time is inversely proportional to the thermal conductance. For a sample placed directly on an AlN substrate, G_s is much larger than it would be on Teflon tape, so we have a much faster response time.

We can conclude that both the amplitude and response time of PV in p-n junction SWCNT films are very sensitive to substrate. The response time of the PV can be enhanced by choosing a good thermal conductor as substrate but at the cost of the decrease of signal amplitude.

4.3.3 The Effect of n-Doping Level on PV Amplitude

As discussed before, PV originates from the sharp change of Seebeck coefficient from the p-type film to the n-type film. It means that the larger the Seebeck coefficient in n-type film by BV doping, the larger the PV signal. So, PV can be affected by the concentration of BV doping. In this section, we discuss the relationship between PV and BV concentration.

A series of BV solutions with different BV concentration were made according to the recipe described in Section 3.3.2. Different SWCNT samples with sharp p-n junctions were made by dropping the same volume (5 µL) of BV solution but with different concentration. Teflon tape was chosen as the substrate for all samples. PV measurements on these samples were performed by focusing light at the junction with power ∼10 mW. Figure 4.11 shows the results.

From Figure 4.11, we can see that the dependence of PV signal on BV concentration is nonlinear. Initially, it increases very fast with the increasing BV concentration,

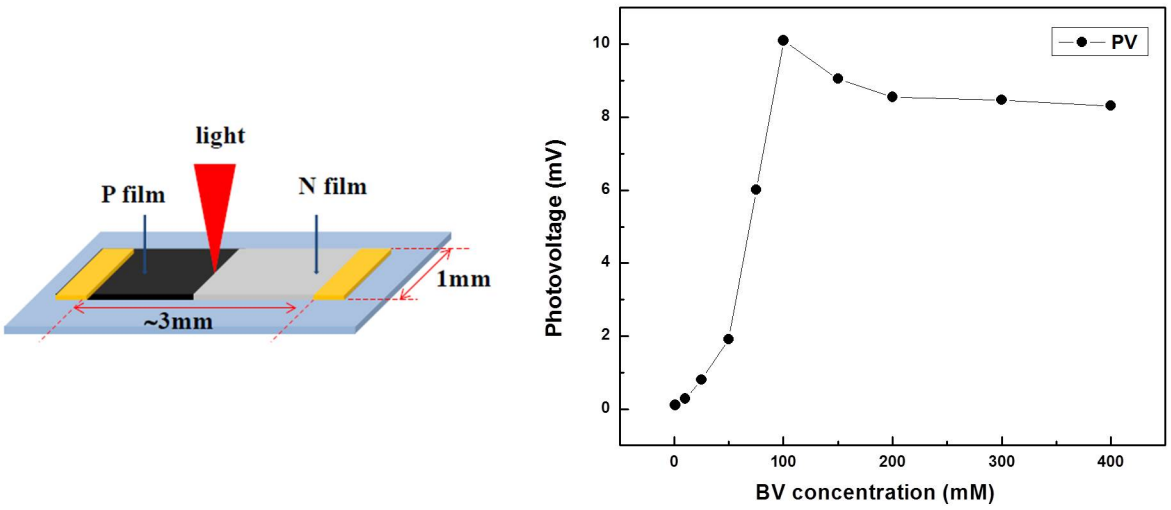

Figure 4.11 : PV as a function of concentration of BV solution. The left insets show the diagram of samples for the measurement.

but it then reaches a maximal value at a concentration of 100 mM. After that, increasing the BV concentration leads to a slight decrease in PV.

This result is explained by taking into account the dependence of Seebeck coefficient on carrier concentration (discussed in Section 4.1). The Seebeck coefficient of semiconducting SWCNTs can be modulated by changing the carrier concentration in the system. It increases fast at low carrier density and reaches a maximum, then starts decreasing with the continuing increase in carrier density (see Figure 4.2). In our experiment, 100 mM is the concentration at which the carrier density of the SWCNT films has reached the optimal value and thus gives a maximal Seebeck coefficient. As a result, the PV signal reaches a maximum.

We conclude that PV signal is strongly dependent on doping level, which can be controlled by the concentration of doping solution. The maximal PV signal can be

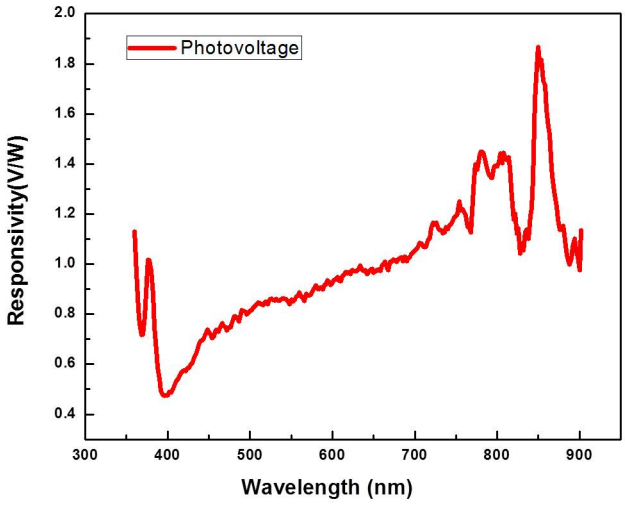

Figure 4.12 : Responsivity (normalized PV) from 360–900 nm for p-n junction SWCNT samples at room temperature.

achieved by optimizing the n or p-doping level of SWCNT films.

4.4 Broadband PV Measurements on p-n Junction Samples

It is known that semiconducting CNTs can absorb light in a very broad range due to the polydisperity of their diameters. This is one of the advantages of SWCNTs in the potential application in opto-electronic devices. Our ultimate goal on the study of p-n junction SWCNT samples is to design a broadband photodetector. So it is necessary to check their photoresponse in a wide wavelength range. In this section, we discuss the PV of our samples in a wide wavelength range.

The sample we used here was grown by CVD, and the n-type film was doped by BV solution with the optimal concentration of 100 mM. A sharp p-n junction was made between the p-type film and the n-type film that were supported by Teflon

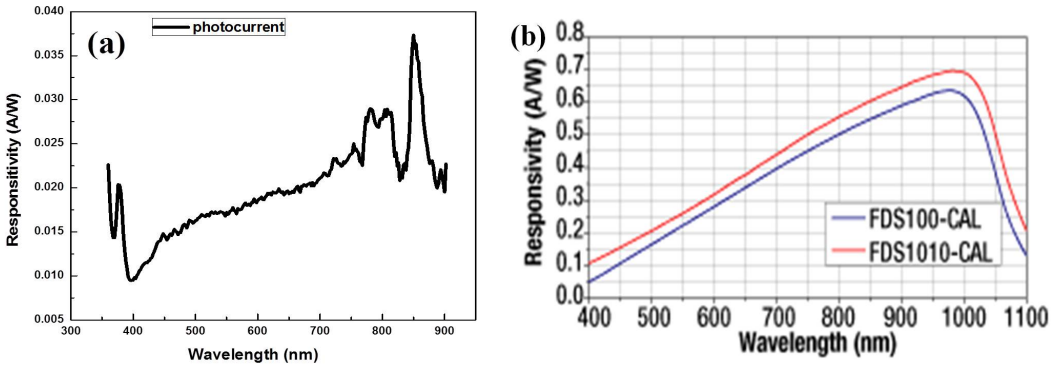

Figure 4.13 : (a) Responsivity of *p*-*n* junction SWCNT samples. (b) Responsivity of Si photodiode (Thorlabs Inc.).

tape. The measurement was performed in a free standing situation (without glass slides). In order to check PV in a wide wavelength range, a UV enhanced Xe lamp was used as a light source with an average power of ∼1 mW. Figure 4.12 shows PV dependence on wavelength in the range 360–900 nm, in which PV signal has been normalized by illumination power and characterized as responsivity. We found that our samples generated PV in the entire range. It increases steeply toward the UV range and increases slowly toward the infrared.

We also made the comparison between our *p*-*n* junction CNT sample and a commercial Si photo detector. PV data was converted into photocurrent by dividing out the sample resistance ∼50 Ω. Although it has photoresponse in the entire wavelength range, the responsivity of *p*-*n* junction SWCNT samples is lower than that of Si photodetector by one order of magnitude. So in order to compete with commercial devices, the responsivity of our samples need to be increased.

According to the above experiment, we can conclude that *p*-*n* junction SWCNT samples generate PV in the full visible range. However, currently, its responsivity is

too low to compete with Si photodetectors in this range. For commercial applications, the responsivity needs to be largely improved, and also it is necessary to check its response in a longer wavelength range.

Chapter 5

Summary

Vertically aligned SWCNTs with length around 60 µm were grown by CVD and transferred to different substrates. These include Teflon tape wrapped around a glass slide, pure Teflon tape, and AlN thin films. n-doped SWCNT films were made by BV-doping with different doping concentration. Then p-n junctions were fabricated by slightly overlapping one unintentionally p-doped film with another n-doped film.

Scanning PV measurements were performed on p, n and p-n junction samples by illumination with a 660 nm laser diode. PV was observed on all kinds of samples under the same illumination power ∼10 mW. An obvious shift was observed in I-V curve but without a rectifying effect, implying that there was not a depletion region in the p-n junction sample. It was mainly due to the mixture of metallic and semiconducting SWCNTs in samples grown by CVD. So the observed PV was attributed to the PTE effect. For p and n-type samples, PV only appeared at two metallic electrode-SWCNT interfaces. It changed sign at the same interface from p to n sample, indicating the transition from p to n-type by BV doping and so sign change of Seebeck coefficient. For p-n junction samples, the PV observed at the junction was larger by one order of magnitude than the signal at metallic electrode-SWCNT interfaces contributed by a sharp change of Seebeck coefficient from p to n-type films.

Various factors affecting PV amplitude and response time were studied, including the length of the overlapping region, different substrates, and doping concentration. It was found that PV is generated at the edge of the p-n junction, the overlapping

region behaves like one intrinsic semiconducting SWCNT film with near zero Seebeck coefficient because of the small temperature gradient along the perpendicular direction. It was also found that substrates can affect both PV response time and amplitude through heat dissipation. The maximal PV amplitude of around 1 V/W was observed with samples on Teflon tape but with very slow response times on the order of a few seconds. The fastest response time of ∼80 µs was observed in samples on AlN substrates but with a small PV amplitude of ∼0.5 V/W. This indicates that PV response times can be enhanced by choosing a good thermal conductor as a substrate but at the cost of its amplitude.

PV measurement on samples with different doping concentrations showed that PV is nonlinearly dependent on the doping level. The maximal PV can be achieved by optimizing both the n and p-doping levels of SWCNT films. PV measurement at different wavelengths showed that the sample has a response in the entire visible range, but its responsivity is too low to compete with Si photodetectors in this range. For commercial application, the responsivity must be largely improved, and also it is necessary to check its response in a longer wavelength range.

There are two possible ways to improve the performance of photodetectors based on p-n junction SWCNT films. First, using photolithography to make many microscopic p-n junctions in one SWCNT film and connect them in series, which can increase the PV amplitude. Second, using ultralong SWCNTs to make films instead of short length SWCNTs; in doing so, PV response time can be increased.

Bibliography

[1] S. Iijima. Helical microtubules of graphitic carbon. *Nature*, 354:56–58, 1991.

[2] Phaedon Avouris, Marcus Freitag, and Vasili Perebeinos. Carbon-nanotube photonics and optoelectronics. *Nature Photon.*, 2:341–359, 2008.

[3] T. Hasan F. Bonaccorso, Z. Sun and A. C. Ferrari. Graphene photonics and optoelectronics. *Nature Photon.*, 4:611–622, 2010.

[4] F. Léonard. *The physics of Carbon Nanotube Devices*. William-Andrew, 2008.

[5] Robert J. Chen, Nathan R. Franklin, Jing Kong, Jien Cao, and Thomas W. Tombler. Molecular photodesorption from single-walled carbon nanotubes. *Appl. Phys. Lett.*, 79:2258, 2001.

[6] Moonsub Shim and Giles P. Siddons. Photoinduced conductivity changes in carbon nanotube transistors. *Appl. Phys. Lett.*, 83:3564, 2003.

[7] I. A. Levitsky and W. B. Euler. Photoconductivity of single-wall carbon nanotubes under continuous-wave near-infrared illumination. *Appl. Phys. Lett.*, 83:1857, 2003.

[8] M. Freitag, Y. Martin, J. A. Misewich, R. Martel, and Phaedon Avouris. Photoconductivity of single carbon nanotubes. *Nano Lett.*, 3:1067–1071, 2003.

[9] A. Mohite, S. Chakraborty, P. Gophinath, G. U. Sumanasekera, and B. W.

Alphenaar. Displacement current detection of photoconduction in carbon nanotubes. *Appl. Phys. Lett.*, 86:061114, 2005.

[10] D.H. Lien, W.K. Hsu, H.W. Zan, N.H. Tai, and C.H. Tsai. Photocurrent amplification at carbon nanotubemetal contacts. *Adv. Mater.*, 18:98–103, 2006.

[11] Jia-Lin Sun, Jinquan Wei, Jia-Lin Zhu, Dong Xu, Xiaomeng Liu, Hongsan Sun, De-Hai Wu, and Nian-Le Wu. Photoinduced currents in carbon nanotube/metal heterojunctions. *Appl. Phys. Lett.*, 88:131107, 2006.

[12] Shaoxin Lu and Balaji Panchapakesan. Photoconductivity in single wall carbon nanotube sheets. *Nanotechnology*, 17:1843–1850, 2006.

[13] Mikhail E. Itkis, Ferenc Borondics, Aiping Yu, and Robert C. Haddon. Bolometric infrared photoresponse of suspended single-walled carbon nanotube films. *Science*, 312:413–416, 2006.

[14] Ashkan Benham, Jason L. Johnson, Yongho Choi, M. Günhan Ertosun, Ali K. Okyay, Pawan Kapur, Krishna C. Saraswat, and Ant Ural. Experimental characterization of single-walled carbon nanotube film-si schottky contacts using metal-semiconductor-metal structures. *Appl. Phys. Lett.*, 92:243116, 2008.

[15] Basudev Pradhan, Kristina Setyowati, Haiying Liu, David H. Waldeck, and Jian Chen. Carbon nanotubepolymer nanocomposite infrared sensor. *Nano Lett.*, 8:1142–1146, 2008.

[16] Christopher A. Merchant and Nina Markovic. Effects of diffusion on photocurrent generation in single-walled carbon nanotube films. *Appl. Phys. Lett.*, 92:243510, 2008.

[17] Paul Stokes, Liwei Liu, Jianhua Zou, Lei Zhai, Qun Huo, and Saiful I. Khondaker. Photoresponse in large area multiwalled carbon nanotube/polymer nanocomposite films. *Appl. Phys. Lett.*, 94:042110, 2009.

[18] Benoit C. St-Antoine, David Ménard, and Richard Martel. Position sensitive photothermoelectric effect in suspended single-walled carbon nanotube films. *Nano. Lett.*, 9:3503, 2009.

[19] Lin Xiao, Yuying Zhang, Yang Wang, Kai Liu, Zheng Wang, Tianyi Li, Zhe Jiang, Junpeng Shi, Liang Liu, QunQing Li, Yonggang Zhao, Zhenghe Feng, Shoushan Fan, and Kaili Jiang. A polarized infrared thermal detector made from super-aligned multiwalled carbon nanotube films. *Nanotechnology*, 22:025502, 2011.

[20] M. Omari and N. A. Kouklin. Photothermovoltaic effect in carbon nanotubes: En route toward junctionless infrared photocells and light sensors. *Appl. Phys. Lett.*, 98:243113, 2011.

[21] Kannan Balasubramanian, Yuwei Fan, Marko Burghard, Klaus Kern, Marcel Friedrich, Uli Wannek, and Alf Mews. Photoelectronic transport imaging of individual semiconducting carbon nanotubes. *Appl. Phys. Lett.*, 84:2400, 2004.

[22] Ji Ung Lee. Photovoltaic effect in ideal carbon nanotube diodes. *Appl. Phys. Lett.*, 87:073101, 2005.

[23] Kannan Balasubramanian, Marko Burghard, Klaus Kern, Matteo Scolari, and Alf Mews. Photocurrent imaging of charge transport barriers in carbon nanotube devices. *Nano Lett.*, 5:507–510, 2005.

[24] Marcus Freitag, James C. Tsang, Ageeth Bol, Dongning Yuan, Jie Liu, and Phaedon Avouris. Imaging of the schottky barriers and charge depletion in carbon nanotube transistors. *Appl. Phys. Lett.*, 7:2037–2042, 2007.

[25] Ji Ung Lee, Peter J. Codella, and Matthew Pietrzykowski. Direct probe of excitonic and continuum transitions in the photocurrent spectroscopy of individual carbon nanotube p-n diodes. *Appl. Phys. Lett.*, 90:053103, 2007.

[26] Nathaniel M. Gabor, Zhaohui Zhong, Ken Bosnick, Jiwoong Park, and Paul L. McEuen. Extremely efficient multiple electron-hole pair generation in carbon nanotube photodiodes. *Science*, 325:1367, 2009.

[27] Kenji Hata, Don N. Futaba, Kohei Mizuno, Tatsunori Namai, Motoo Yumura, and Sumio Iijima. Water-assisted highly efficient synthesis of impurity-free single-walled carbon nanotubes. *Science*, 306:1362, 2004.

[28] Jinquan Wei, Yi Jia, Qinke Shu, Zhiyi Gu, Kunlin Wang, Daming Zhuang, Gong Zhang, Zhicheng Wang, Jianbin Luo, Anyuan Cao, and Dehai Wu. Double-walled carbon nanotube solar cells. *Nano Lett.*, 7:2317–2321, 2007.

[29] Yi Jia, Jinquan Wei, Kunlin Wang, Anyuan Cao, Qinke Shu, Xuchun Gui, Yanqiu Zhu, Daming Zhuang, Gong Zhang, Beibei Ma, Liduo Wang, Wenjin Liu, Zhicheng Wang, Jianbin Luo, and Dehai Wu. Nanotube-silicon heterojunction solar cells. *Adv. Mater.*, 20:4594, 2008.

[30] Michael S. Arnold, Jeramy D. Zimmerman, Christopher K. Renshaw, Xin Xu, Richard R. Lunt, Christine M. Austin, and Stephen R. Forrest. Broad spectral response using carbon nanotube/organic semiconductor/c_{60} photodetectors. *Nano Lett.*, 9:3354, 2009.

[31] Zhongrui Li, Vasyl P. Kunets, Viney Saini, Yang Xu, Enkeleda Dervishi, Gregory J. Salamo, Alexandru R. Biris, and Alexandru S. Biris. Light-harvesting using high density p-type single wall carbon nanotube/n-type silicon heterojunctions. *ACS Nano*, 3:1407, 2009.

[32] Ye Liu, Shaoxin Lu, and Balaji Panchapakesan. Alignment enhanced photoconductivity in single wall carbon nanotube films. *Nanotechnology*, 20:035203, 2009.

[33] Dominick J. Bindl, Nathaniel S. Safron, and Michael S. Arnold. Dissociating excitons photogenerated in semiconducting carbon nanotubes at polymeric photovoltaic heterojunction interfaces. *ACS Nano*, 4:5657, 2010.

[34] Dominick J. Bindl, Meng-Yin Wu, Frederick C. Prehn, and Michael S. Arnold. Efficiently harvesting excitons from electronic type-controlled semiconducting carbon nanotube films. *Nano Lett.*, 11:455, 2011.

[35] Sebastien Nanot, Cary L. Pint, Akira Ikeuchi, Takafumi Akiho, Kazuhisa Sueoka, Aron Cummings, Robert H. Hauge, Francois Leonoard, and Junichiro Kono. Polarization-sensitive photodetector based on optically-thick films of macroscopically long, dense, and aligned carbon nanotubes. *Nature Photonics, preprint.*

[36] R. Martel, V. Derycke, C. Lavoie, J. Appenzeller, K. K. Chan, J. Tersoff, and Phaedon Avouris. Ambipolar electrical transport in semiconducting single-wall carbon nanotubes. *Phys. Rev. Lett.*, 87:256805, 2001.

[37] Cary L. Pint. *Synthesis, transfer printing, electrical and optical properties, and applications of materials composed of self-assembled, aligned single-walled carbon nanotubes.* PhD thesis, Rice University, 2010.

[38] R. F. Wood, S. Pannala, J. C. Wells, A. A. Puretzky, and D. B. Geohegan. Simple model of the interrelation between single- and multiwall carbon nanotube growth rates for the cvd process. *Phys. Rev. B*, 75:235446, 2007.

[39] S. Noda, K. Hasegawa, H. Sugime, K. Kakehi, Z. Zhang, S. Maruyama, and Y. Yamaguchi. Millimeter-thick single-walled carbon nanotube forests: hidden role of catalyst support. *Jpn. J. Appl. Phys.*, 46:L399–L401, 2007.

[40] Placidus B. Amama, Cary L. Pint, Laura McJilton, Seung Min Kim, Eric A. Stach, P. Terry Murray, Robert H. Hauge, and Benji Maruyama. Role of water in super growth of single-walled carbon nanotube carpets. *Nano Lett.*, 9:44, 2009.

[41] Philip G. Collins, Keith Bradley, Masa Ishigami, and A. Zettl. Extreme oxygen sensitivity of electronic properties of carbon nanotubes. *Science*, 287:1801, 2000.

[42] Jessica Campos-Delgado, Indhira O. Maciel, David A. Cullen, David J. Smith, Ado Jorio, Marcos A. Pimenta, Humberto Terrones, and Mauricio Terrones. Chemical vapor deposition synthesis of n-, p-, and si-doped single-walled carbon nanotubes. *ACS Nano*, 4:1696, 2010.

[43] A. L. Elías, P. Ayala, A. Zamudio, M. Grobosch, E. Cruz-Silva, J. M. Romo-Herrera, J. Campos-Delgado, H. Terrones, T. Pichler, and M. Terrones. Spectroscopic characterization of n-doped single-walled carbon nanotube strands: an x-ray photoelectron spectroscopy and raman study. *J. Nanoscience Nanotechnol.*, 10:3959, 2010.

[44] V. Derycke, R. Martel, J. Appenzeller, and Ph. Avouris. Controlling doping and carrier injection in carbon nanotube transistors. *Appl. Phys. Lett.*, 80:2773, 2002.

[45] Yangxin Zhou, Anshu Gaur, Seung-Hyun Hur, Coskun Kocabas, Matthew A. Meitl, Moonsub Shim, and John A. Rogers. p-channel, n-channel thin film transistors and pn diodes based on single wall carbon nanotube networks. *Nano. Lett.*, 4:2031–2035, 2004.

[46] Giles P. Siddons, David Merchin, Ju Hee Back, Jae Kyeong Jeong, and Moonsub Shim. Highly efficient gating and doping of carbon nanotubes with polymer electrolytes. *Nano. Lett.*, 4:927–931, 2004.

[47] Soo Min Kim, Jin Ho Jang, Ki Kang Kim, Hyeon Ki Park, Jung Jun Bae, Woo Jong Yu, Il Ha Lee, Gunn Kim, Duong Dinh Loc, Un Jeong Kim, Eun-Hong Lee, Hyeon-Jin Shin, Jae-Young Choi, and Young Hee Lee. Reduction-controlled viologen in bisolvent as an environmentally stable n-type dopant for carbon nanotubes. *J. Am. Chem. Soc.*, 131:327–331, 2009.